J. Am. Ceram. Soc., 1–9 (2016)
DOI: 10.1111/jace.14589

journal

Composition and Temperature Dependence of Structure and Piezoelectricity in $(1-x)(K_{1-y}Na_y)NbO_3$-$x(Bi_{1/2}Na_{1/2})ZrO_3$ Lead-Free Ceramics

Dawei Wang,[‡,§] Fayaz Hussain,[‡] Amir Khesro,[‡] Antonio Feteira,[¶] Ye Tian,[‖] Quanliang Zhao,[§] and Ian M. Reaney[‡,†]

[‡]Department of Materials Science and Engineering, University of Sheffield, Sheffield S1 3JD, UK

[§]Department of Materials Science and Engineering, North China University of Technology, Beijing 100144, China

[¶]Christian Doppler Laboratory for Advanced Ferroic Oxides, Sheffield Hallam University, Sheffield S1 1WB, UK

[‖]School of Engineering and Materials Science, Queen Mary University of London, London E1 4NS, UK

Lead-free piezoceramics with the composition $(1-x)(K_{1-y}Na_y)NbO_3$-$x(Bi_{1/2}Na_{1/2})ZrO_3$ (KNyN-xBNZ) were prepared using a conventional solid-state route. X-ray diffraction, Raman spectroscopy, and dielectric measurements as a function of temperature indicated the coexistence of rhombohedral (R) and tetragonal (T) phase, typical of a morphotropic phase boundary (MPB) as the BNZ concentration increased and by adjusting the K/Na ratio. High remnant polarization (P_r = 24 μC/cm^2), piezoelectric coefficient (d_{33} = 320 pC/N), effective piezocoefficient (d^*_{33} = 420 pm/V), coupling coefficient (k_p = 48%), and high strain (S = 0.168%) were obtained at room temperature, but significant deterioration of P_r, d^*_{33}, and k_p were observed by increasing from room temperature to 160°C (17.5 μC/cm^2, 338 pm/V, and 32%, respectively) associated with a transition to a purely T phase. Despite these compositions showing promise for room-temperature applications, the deterioration in properties as a function of increasing temperature poses challenges for device design and remains to be resolved.

Keywords: *lead-free ceramics; piezoelectric materials/properties; potassium-sodium niobate/KNN*

I. Introduction

PIEZOELECTRIC materials have being extensively investigated because of their widespread applications ranging from medical, environmental, and industrial process monitoring to robotics, energy harvesting, and high-frequency communication systems.[1,2] Most commonly used materials are based on lead zirconate titanate $Pb(Zr,Ti)O_3$ (PZT) due to their high piezoelectric performance.[3–5] However, regulations against hazardous substances such as lead in electric and electronic equipment has stimulated research in lead-free piezoelectrics over the last two decades.[6–14]

Potassium-sodium niobate $(K,Na)NbO_3$ (KNN) is one of the leading candidates to replace PZT and has been extensively investigated due to its moderately large piezoelectric coefficient (d_{33}) and high Curie temperature (T_C),[15,16] since its discovery in the 1950s.[17] In particular, research on KNN accelerated when Saito et al. (2004) reported giant $d_{33} \sim$ 416 pC/N, comparable to those of PZTs, in textured (Li,Ta, Sb)-modified KNN,[18,19] However, disadvantages such as attaining well-densified ceramics due to the high volatility of the alkaline components and low piezoelectric properties in polycrystalline ceramics have prevented KNN being commercialized.[20–24] In general, dopants in KNN enhance piezoelectricity (d_{33} > 200 pC/N) by pushing the orthorhombic (O) to tetragonal (T) transition boundaries closer to room temperature.[25–44] This effect is well documented for dopants such as $LiSbO_3$, $LiTaO_3$, $Bi_{0.5}Na_{0.5}TiO_3$, and $BaTiO_3$.[25–32] But coexistence of rhombohedral (R) and O phases has been reported for dopants with the general formula $AZrO_3$ (A=Ba, Sr, or Ca) or $BiMO_3$ (M=Fe, Sc, Co).[33–38] Compositions which rely on R-O coexistence generally, however, exhibit $d_{33} \leq 230$ pC/N that are significantly lower the compositions which utilize the O-T phase boundary to optimize d_{33}.

Recently, PZT-like morphotropic phase boundary (MPBs) (R-T) have been reported in KNN-based ceramics by integrating compositions which were previously used to optimize the O-T and R-O phase boundaries.[39–50] In 2011, Zuo et al. reported R-T phase coexistence in (Li,Ta,Sb) and $BaZrO_3$ multimodified KNN lead-free ceramics and obtained a high d_{33} = 365 pC/N.[39–41] For similar compositions, Wu et al. obtained $d_{33} \sim$ 425 pC/N.[42] But more recently, Sb together with $(Bi,M)NO_3$ (M=Na, K, Li, Ag, N=Zr, Hf, Sn) have been used to enhance d_{33} and electromechanical strain (S) with d_{33} and S improved to >400 pC/N and 0.46% at 3 kV/cm, respectively.[43–49] Despite promising d_{33} and S values there are still a number of concerns. For Sb doping, T_C is reported to decrease alarmingly and de-poling may jeopardize some applications. More importantly, however, to our knowledge, the temperature dependence of the piezoelectric properties is rarely reported. It is likely that the supposed MPB in many KNN-based compositions is not temperature independent and therefore phase coexistence and high d_{33}/S are not maintained during high-temperature applications or at high field cyclic loading in which temperature is likely to increase. Given the above concerns, this contribution presents the composition and temperature dependence of the piezoelectric properties $(1-x)(K_{1-y}Na_y)NbO_3$-$x(Bi_{1/2}Na_{1/2})ZrO_3$ (KNyN-xBNZ) lead-free ceramics in which $LiSbO_3$ dopants have been excluded to maintain a high T_C.

II. Experimental Procedure

The KNyN-xBNZ ceramics with compositions of $(1-x)(K_{1-y}Na_y)NbO_3$-$x(Bi_{1/2}Na_{1/2})ZrO_3$ (x = 0, 0.02, 0.03, 0.04, 0.045, 0.05, 0.06, 0.08, and y = 0.6) and (x = 0.045, and y = 0.4, 0.45, 0.49, 0.53, 0.56, 0.6, 0.65, and 0.7) were prepared using a conventional solid-state reaction. Raw materials, including Na_2CO_3 (99.9%, Fisher Scientific), K_2CO_3

S. Zhang—contributing editor

Manuscript No. 38841. Received July 8, 2016; approved September 8, 2016.
†Author to whom correspondence should be addressed. e-mail: i.m.reaney@sheffield.ac.uk

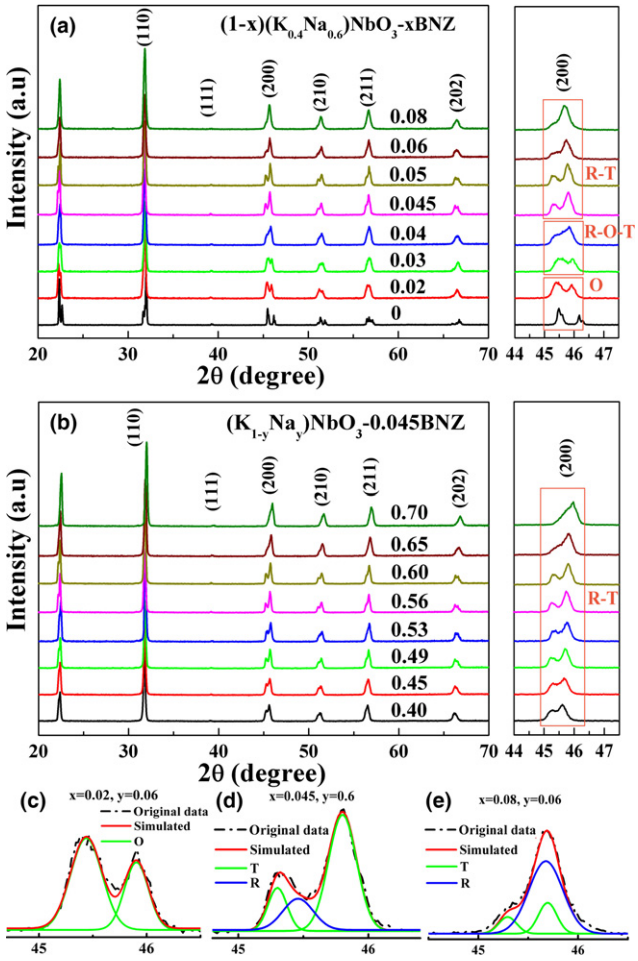

Fig. 1. Room temperature XRD patterns of KNyN-xBNZ (a) KN0.6N-xBNZ and (b) KNyN-0.045BNZ; amplified XRD patterns simulated by Gaussian for (c) KN0.06N-0.02BNZ (d) KN0.06N-0.045BNZ (e) KN0.06N-0.08BNZ.

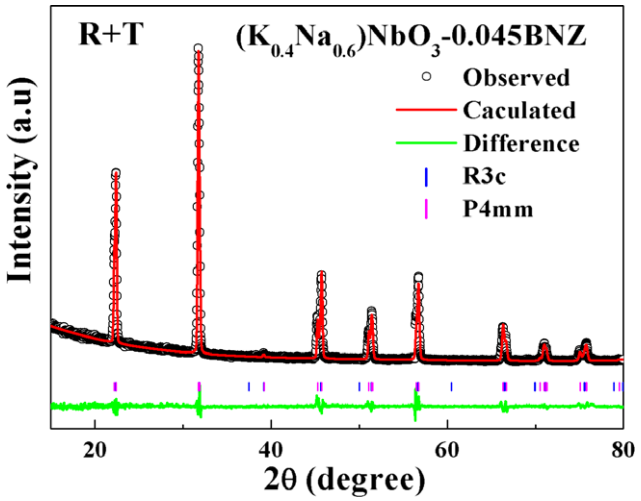

Fig. 2. Rietveld refinement analysis of KN0.6N-0.045BNZ using the GSAS+EXPGUI package. Two phases *R3c* + *P4 mm* were used. R_p = 6.2%, R_{wp} = 9.7% and χ^2 = 1.88.

(99.7%, Fisher Scientific), Nb_2O_5 (99.5%, Sigma-Aldrich), ZrO_2 (99%, Sigma-Aldrich), and Bi_2O_3 (99.9%, Sigma-Aldrich) were batched stoichiometrically according to the nominal compositions and ball-milled in isopropanol for 24 h. The dried mixed powders were calcined at 850°C for 6 h to synthesize the compound and then ball milled in isopropanol

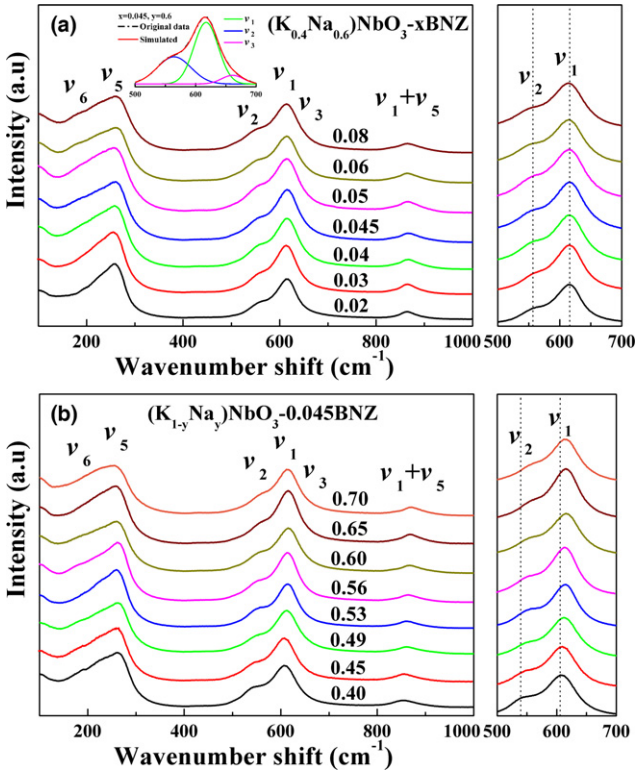

Fig. 3. Room temperature Raman spectra of KNyN-xBNZ (a) KN0.6N-xBNZ, inset shows the Raman amplified peaks around 600 cm^{-1} simulated by Gaussian and (b) KNyN-0.045BNZ.

for 12 h. The calcined powders were mixed with a polyvinyl alcohol (PVA) binder solution, granulated and pressed into pellets with 10 mm in diameter. Following binder burnout at 550°C, the pellets were sintered in a sealed crucible with sacrificial powders at 1150°C–1230°C for 3–6 h.

The density of the sintered samples was measured by the Archimedes method. The relative density of all studied samples was higher than 95%. The phase structure of the sintered samples was studied using a Bruker D2 Phaser X-ray powder diffraction (XRD) and *in situ* XRD performed for selected samples using a Siemens D5000 HTXRD in the temperature range 30°C–350°C. Ceramic morphology and microstructure was examined using an FEI Inspect F scanning electron microscope (SEM). Raman spectra were acquired from −150°C to 350°C using a Renishaw inVia Raman microscope. For electrical tests, sintered samples were electroded using fire-on silver paste, followed by the samples being poled in silicon oil at room temperature with an applied electric field of 30–40 kV/cm. Piezoelectric coefficient (d_{33}) was measured using a Piezotest PM300 d_{33} meter. Polarization hysteresis and strain-electric field behavior were determined using an aixACCT TF 2000 ferroelectric tester at a frequency of 1 Hz from room temperature to 160°C. The displacement data were synchronously captured by a laser interferometer. The temperature-dependent dielectric permittivity from 25°C to 600°C was measured using an Agilent 4184A multifrequency precision LCR meter. The planar electromechanical coupling factor (k_p) was determined from the resonance and antiresonance frequencies, which were measured using an Agilent 4294A Impedance/Gain-phase analyzer according to IEEE standards on piezoelectricity.[51,52]

III. Results and Discussion

(1) Compositional Evolution of Structure–Property Relations

The room-temperature XRD patterns of KNyN-xBNZ in the 2θ range of 20°–70° are shown in Fig. 1. All peaks

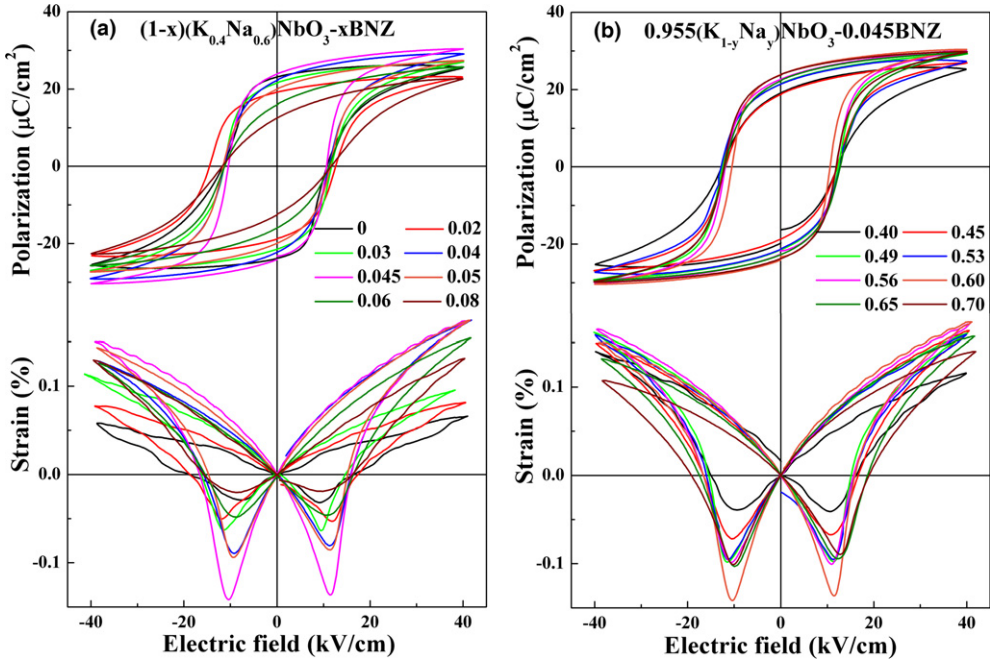

Fig. 4. High electric field bipolar polarization hysteresis and strain loops for KNyN-xBNZ (a) KN0.6N-xBNZ and (b) KNyN-0.045BNZ.

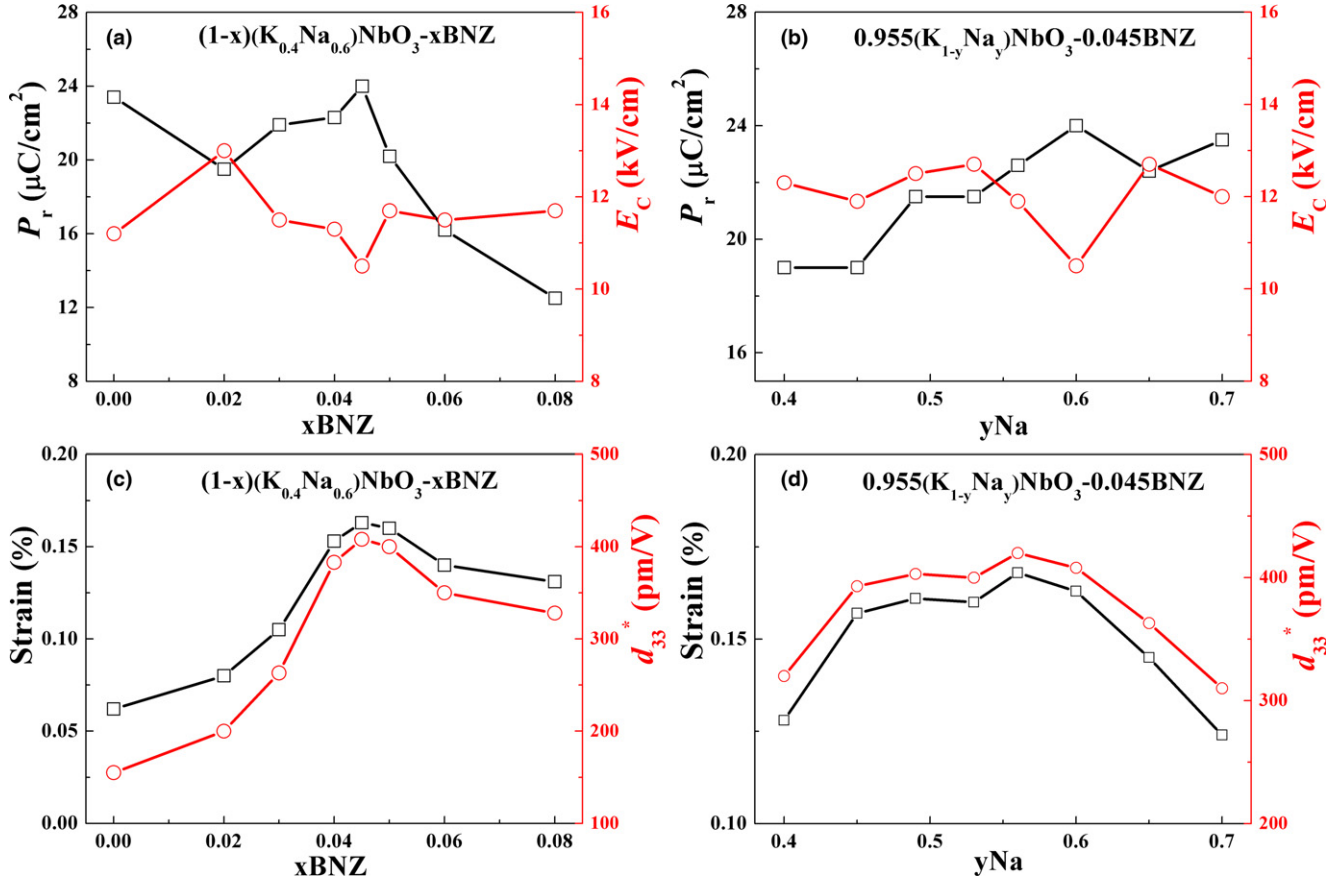

Fig. 5. Ferroelectric and strain properties of KNyN-xBNZ (a) P_r and E_C as a function of BNZ, (b) P_r and E_C as a function of Na, (c) S and d^*_{33} as a function of BNZ, (d) S and d^*_{33} as a function of Na.

could be attributed to perovskite phases, indicating that a stable solid solution was formed in the studied range. Diffraction peaks shifted to a lower and higher diffraction angle with increasing BNZ and Na concentration, respectively, consistent with differences in relative ionic radius of the dopant/substituent ions with the matrix composition. Splitting of (200) peak at ~2θ = 45° was used to determine the likely symmetry of compositions. In the expanded XRD patterns [Fig. 1(a)], O phase was dominant in KN0.6N-xBNZ with $x \leq 0.02$, but R, O and T phases coexisted for compositions of $0.03 \leq x \leq 0.04$. As x increased further, ceramics with $0.045 \leq x \leq 0.05$ showed mixed R and T

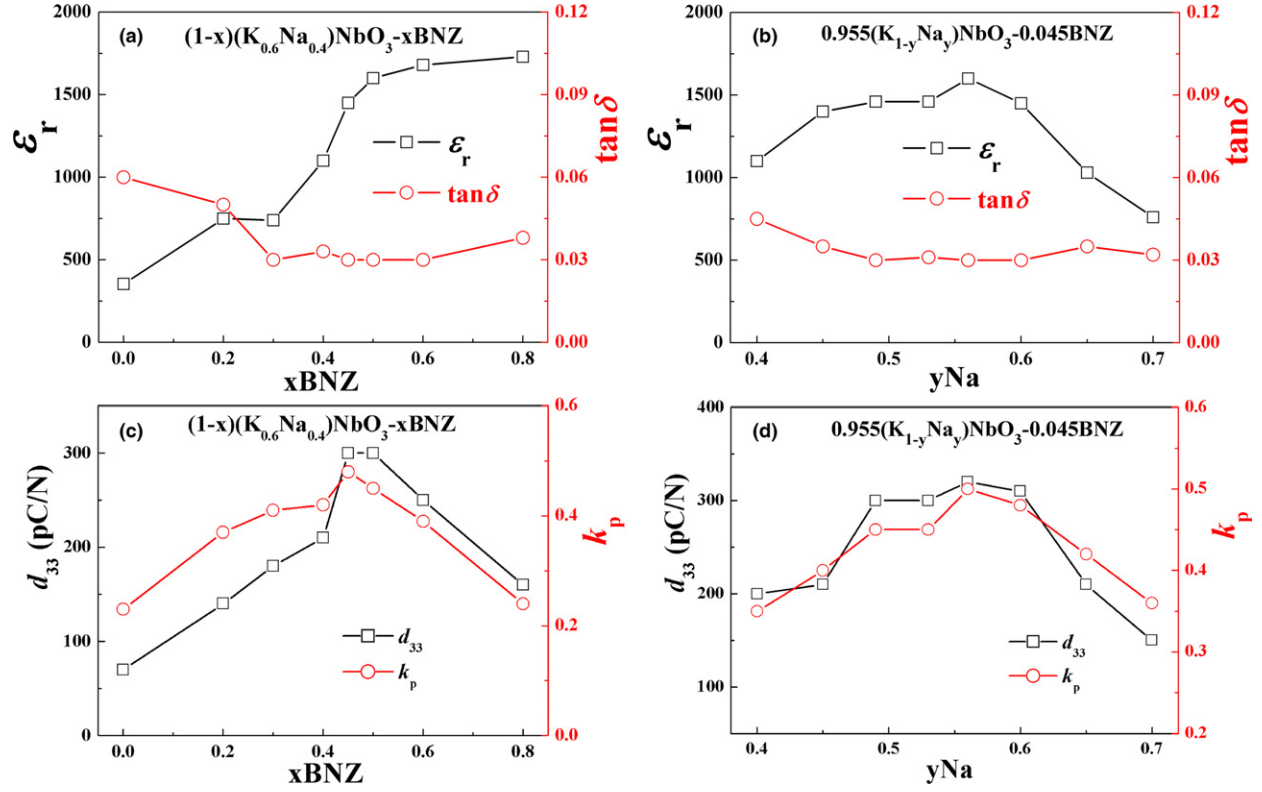

Fig. 6. Dielectric and piezoelectric properties of KNyN-xBNZ (a) ε_r and tanδ as a function of BNZ, (b) ε_r and tanδ as a function of Na, (c) d_{33} and k_p as a function of BNZ, (d) d_{33} and k_p as a function of Na.

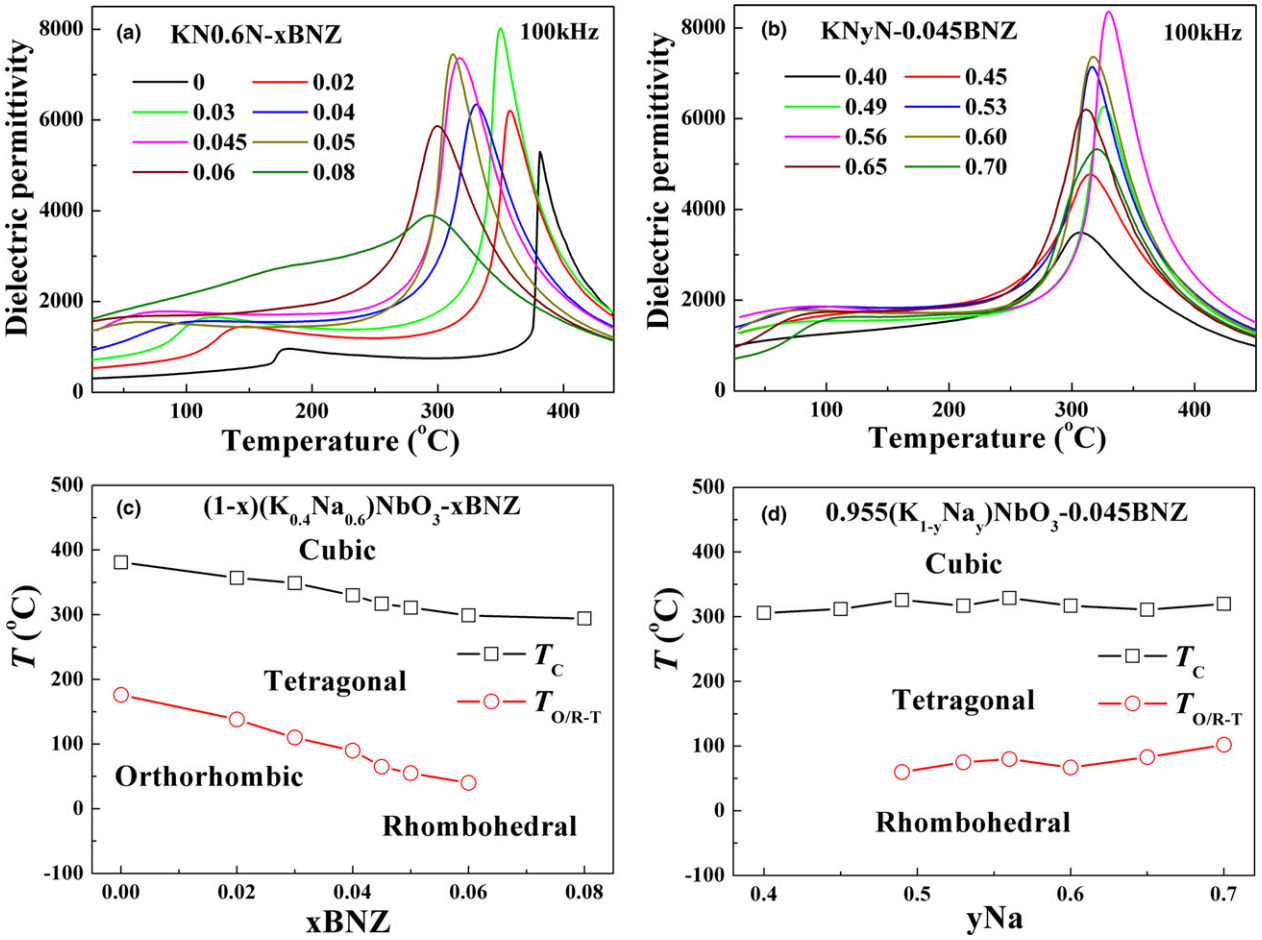

Fig. 7. Temperature dependence of ε_r and tanδ for KNyN-xBNZ (a) KN0.6N-xBNZ, (b) KNyN-0.045BNZ, (c) T_C and $T_{O/R-T}$ as a function of BNZ, (d) (c) T_C and $T_{O/R-T}$ as a function of Na.

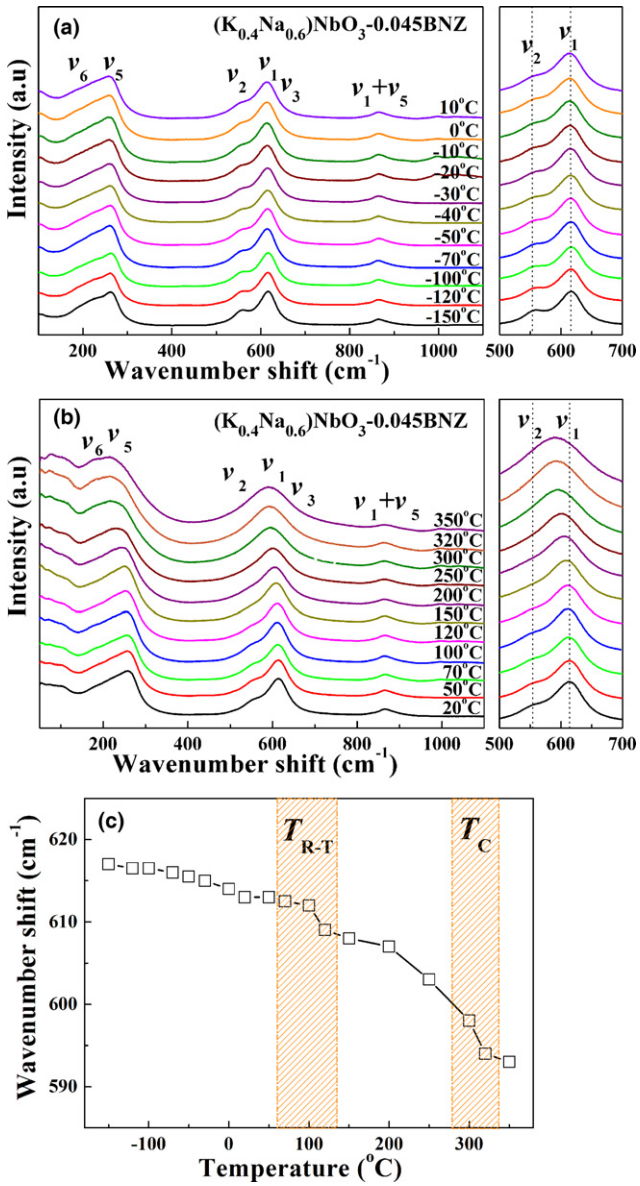

Fig. 8. *In situ* temperature dependence of Raman spectra for KN0.6N-0.045BNZ (a) −150°C–10°C, (b) 20°C–350°C, (c) ν_1 peak shift as a function of temperature.

phases. For $x > 0.05$, a single peak emerged, suggesting that R phase dominated. For compositions in which x was maintained at 0.045 (KNyN-0.045BNZ), the splitting of (200)/(002) peaks gradually disappeared as y increased, suggesting the coexistence of R and T for a wide variation in Na:K ratio, Fig. 1(b). To confirm the phase evolution in KNyN-xBNZ as a function of composition, simulations were performed, Fig. 1(c–e), which are consistent with experimental data and also the interpretation by Wang et al.[43–50] Rietveld refinement analysis of the MPB composition KN0.6N-0.045BNZ was also performed using the GSAS+EXPGUI package,[53,54] where a two phases refinement (*R3c* + *P4 mm*) was used, as shown in Fig. 2. A good agreement between the observed and calculated patterns was obtained with $R_p = 6.2\%$, $R_{wp} = 9.7\%$ and chi-squared (χ^2) = 1.88, indicating the coexistence of R (*R3c*, 32.5%) and T (*P4 mm*, 67.5%) phases in the MPB composition.

To further confirm phase evolution as a function of composition, room-temperature Raman spectra of KNyN-xBNZ ceramics were obtained as shown in Fig. 3. Among the full Raman active mode of KNN, ν_1, ν_2, and ν_3 are stretching modes, ν_5 and ν_6 are bending modes of the NbO_6 octahedra.[55] The strongest peak around 600 cm^{-1} is related to the ν_1 mode; whereas the left and right weaker peaks are assigned to the ν_2 and ν_3 mode, respectively, as indicated by the simulated data shown in the inset of Fig. 3(a). With increasing BNZ content, the ν_1 and ν_2 peaks were found to shift to lower wave number as shown in Fig. 3(a). On the other hand, the ν_1 and ν_2 peaks shift to higher wave number with an increase in Na content as shown in Fig. 3(b). The peak shift to a lower/higher frequency is due to an increase/decrease in binding strength caused by the expansion/shrinkage of the distance between Nb^{5+} and its coordinated oxygen, resulting in the corresponding variation in crystal cell volume.[55,56] However, the clear but gradual symmetry changes observed by XRD were not apparent in the Raman spectra, as evidenced by the absence of the appearance of new symmetry related modes. Raman, however, is not only sensitive to the macroscopic symmetry but is influenced strongly by local distortions to the lattice. It is postulated that within the KNyN-xBNZ system there are compositional regions dominated by "pseudosymmetry" in a manner discussed for La-doped $BiFeO_3$ compositions by Khesro et al.[57] and $Bi_{1/2}(K_{1-x}Na_x)_{1/2}TiO_3$ by Levin and co-workers.[58,59] In these compositions, there are local perturbations in the average macroscopic symmetry more commonly associated with adjacent phases within the phase diagram, for example, short-range antipolar order in the paraelectric phase for La-doped $BiFeO_3$. We propose a similar model for KNyN-xBNZ based on the absence of new symmetry modes in Raman and the gradual changes in peak splitting in XRD but extensive transmission electron microscopy (TEM) work is required before this can be proved conclusively.

The SEM images for the surface of KNyN-xBNZ ceramics (not shown) revealed that the grain size of KN0.6N-xBNZ decreased with increasing BNZ content, from ~5 μm for $x = 0$ and to ~1 μm for $x = 0.08$ but the grain size of KNyN-0.045BNZ was insensitive to the K/Na ratio.

The high electric field bipolar polarization hysteresis and strain loops for KNyN-xBNZ as a function of BNZ and Na content are shown in Fig. 4, from which the remnant polarization (P_r), coercive field (E_C) and average electric field induced strain (S) as a function of BNZ and Na content can be obtained, Fig. 5. The normalized strain coefficient d^*_{33}, representing the average strain per unit of electric field, is calculated by, $d^*_{33} = S_{max}/E_{max}$, where E_{max} is the maximum electric field value, and S_{max} is the average value of the corresponding maximum strain. As shown in Fig. 5(a and b), with increasing BNZ and Na concentration in KNyN-xBNZ, P_r increased and then decreased after reaching a peak value, at which point the lowest E_C was obtained. The highest value of P_r = 24 μC/cm^2 and lowest value of E_C = 10.5 kV/cm was achieved for $x = 0.045$, $y = 0.6$ at the MPB.[60,61] The S and d^*_{33} values increased with increasing BNZ and Na content, reaching maximum values of 0.163%, 408 pm/V at $x = 0.045$, $y = 0.6$ and 0.168%, 420 pm/V at $x = 0.045$, $y = 0.56$, respectively, above which they reduced, Fig. 5(c and d). d^*_{33} is dominated by extrinsic effects, mainly domain wall motion, which the coexistence of R and T phases encourages at the MPB.[61–63]

The dielectric and piezoelectric properties of KNyN-xBNZ as a function of BNZ and Na content are shown in Fig. 6. The room-temperature permittivity (ε_r) of KN0.6N-xBNZ increases with BNZ concentration, whereas it initially increases and then decreases as a function Na/K ratio, Fig. 6(a and b). tanδ initially decreased with BNZ and Na concentration but then became stable for a broad range of compositions, Fig. 6(a and b). d_{33} and k_p both increased significantly with increasing BNZ and Na concentration as shown in Fig. 6(c and d), reaching a maxima of 310 pC/N and 48% for $x = 0.045$, $y = 0.06$, and 320 pC/N and 50% for $x = 0.045$, $y = 0.056$, respectively, and then decreasing for BNZ > 0.05 and Na > 0.6. As with d^*_{33}, d_{33} is optimized at the MPB largely through extrinsic

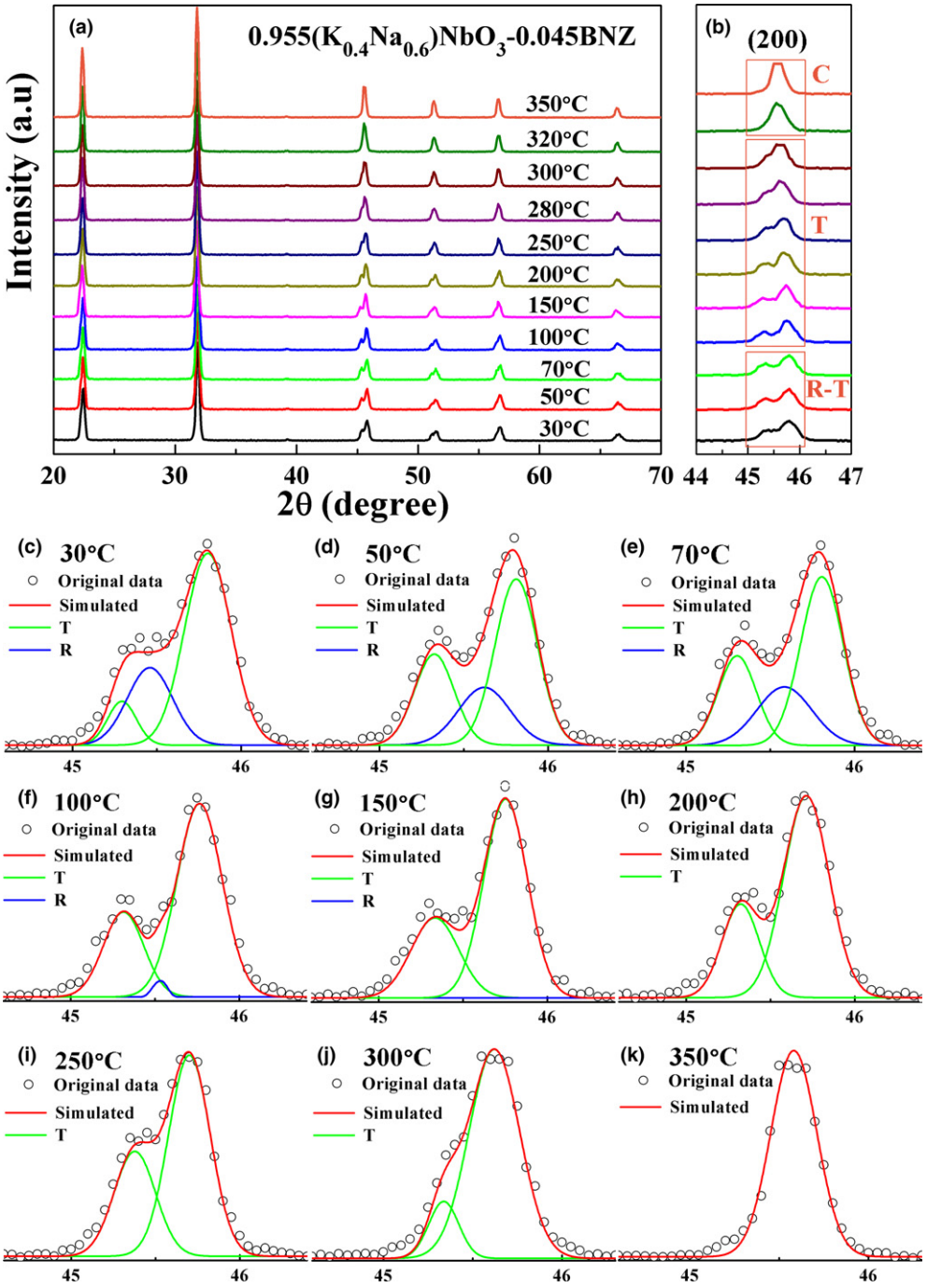

Fig. 9. *In situ* temperature dependence of XRD patterns for KN0.6N-0.045BNZ (a) 2θ = 20°–70°, (b) 2θ = 44°–47°; simulations of splitting of the {200} peaks with different temperatures (c) 30°C, (d) 50°C, (e) 70°C, (f) 100°C, (g) 150°C, (h) 200°C, (i) 250°C, (j) 300°C, and (k) 350°C.

contributions. The facile rotation of the polarization vector between states of similar free energy facilitated by phase coexistence, allows the domain walls to displace reversibly, resulting in a strong extrinsic contribution to the piezoelectric properties.[61,64]

(2) Evolution of Structure–Property Relations as a Function of Temperature

The temperature dependence of dielectric permittivity and loss for KNyN-xBNZ with different BNZ concentration and K/Na ratio is given in Fig. 7. It is well-known that KNN exhibits two dielectric peaks above room temperature, corresponding to the ferroelectric O-T phase transition at ~176°C ($T_{O\text{-}T}$) and the T-cubic (C) phase transition at ~381°C (Curie temperature, T_C). With increasing BNZ concentration, the maximum ε_r at T_C (ε_{max}) increased and T_C decreased continuously, meanwhile, $T_{O\text{-}T}$ decreased and merged with the ferroelectric R-O phase transition ($T_{R\text{-}O}$), resulting in coexistence of R and T phases at room temperature, Fig. 7(a,c), which is consistent with the XRD results (Fig. 1) and previous reports.[43–50] However, T_C remained at ~310°C and $T_{R\text{-}T}$ increased with increasing Na concentration, suggesting the K/Na ratio had little effect on the ferroelectric-paraelectric phase transition of KNyN-xBNZ and that its major influence is on lower temperature transitions. We note also that broad relaxor-like peaks are observed in all compositions if the BNZ concentrations exceeds, $x = 0.08$. Relaxor behavior, however, is not the focus of this study and we note only that KNyN-xBNZ follows trends typically observed in ferroelectric to relaxor compositional transitions with a transformation from a clearly defined macroscopic symmetry

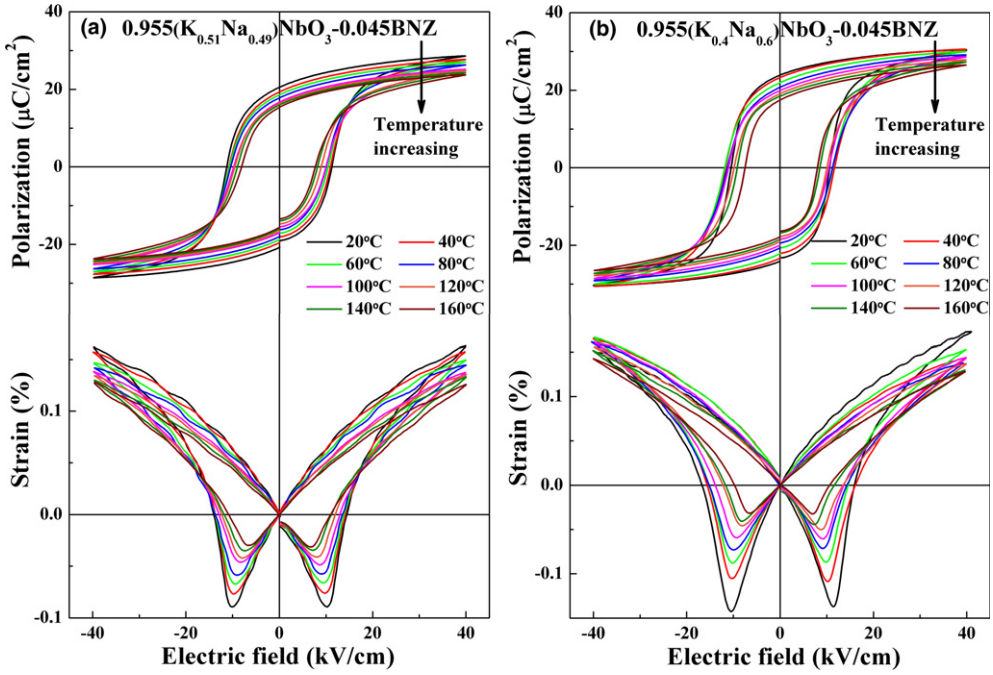

Fig. 10. *In situ* temperature dependence of high electric field bipolar polarization hysteresis and strain loops for two MPB compositions (a) KN0.49N-0.045BNZ and (b) KN0.6N-0.045BNZ.

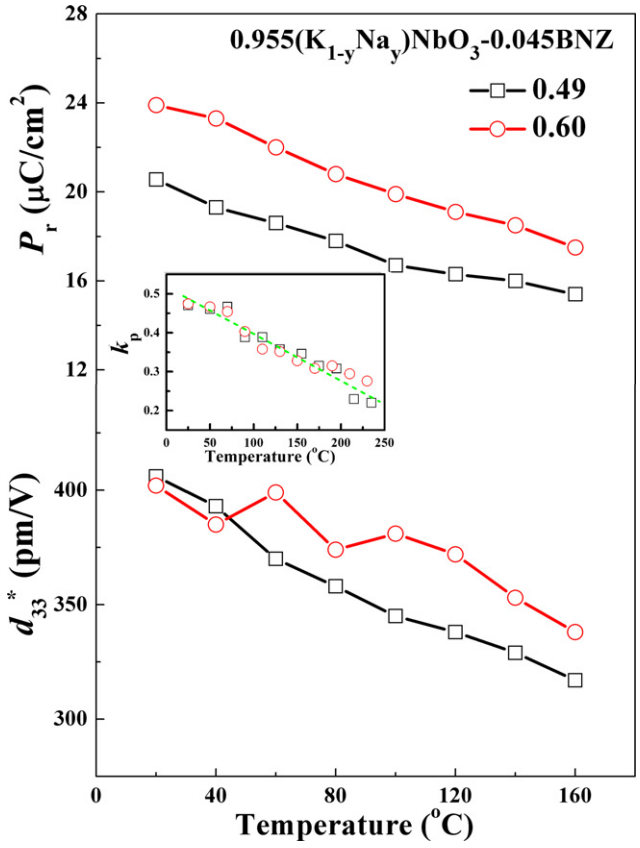

Fig. 11. P_r and d^*_{33} as a function of temperature for KN0.49N-0.045BNZ and KN0.6N-0.045BNZ, inset shows the temperature dependence of k_p.

($x = 0$) to pseudosymmetry ($x > 0.08$) that is associated with loss of long range ferroelectric order through chemical disorder that induces local competition/frustration between phases of similar free energy.

To clarify the structural evolution of KNyN-xBNZ as a function of temperature, *in situ* temperature dependence of Raman and XRD measurements for the selected MPB composition KN0.6N-0.045BNZ were performed, the results from which are plotted in Figs. 8 and 9. As shown in Fig. 8, the general trend is that the ν_1 peak shifted to lower wave number and broadens, accompanied by a gradual fading of the ν_2 peak. More specifically, the ν_1 peak [Fig. 8(c)] revealed a gradual shift in frequency (wave number) up to 70°C–100°C after which there was a sharp change in frequency, coincident with the broad peaks in ε_r at the same temperature range in Fig. 7.

In situ high-temperature XRD data for KN0.6N-0.045BNZ is shown in Fig. 9 which focused on evolution of splitting of the {200} peaks. Phase coexistence was apparent at room temperature as shown by broad multiple peaks that gradually disappeared to become a single peak at high temperatures in the cubic phase. To confirm the phase evolution as a function of temperature, simulations were performed, Fig. 9(c–k). As temperature increased, the coexistence of R-T phases remained up to 70°C–100°C, after which the phase structure total transformed to a T and then C phase above T_C, consistent with experimental ε_r and Raman spectroscopy data as function of temperature.

The *in situ* temperature dependence of high electric field bipolar polarization hysteresis and strain loops for two MPB compositions (KN0.49N-0.045BNZ and KN0.6N-0.045BNZ) are shown in Fig. 10, from which the P_r and d^*_{33} as a function of temperature were obtained, Fig. 11. As temperature increased, P_r and d^*_{33} for both MPB compositions decreased linearly, coincident with a similar temperature dependence of k_p, as shown in the inset of Fig. 11. The piezoelectric effect in ferroelectric ceramics is attributed to both intrinsic (lattice deformation) and extrinsic (domain wall motion) contributions. Normally, P_r reflects intrinsic contribution, and d^*_{33} and k_p contain both components.[40,48] However, detailed knowledge of the domain morphology is required to fully appreciate how the extrinsic contributions is likely to vary as a function of temperature and composition and extensive transmission electron or piezoforce microscopy is required. Nonetheless, the data presented in this contribution clearly illustrates that KNN-BNZ suffers from extreme temperature

dependence which may inhibit its usage in high drive applications and high-temperature applications despite the attractive values of k_p and d_{33} at room temperature.

IV. Conclusion

In this work, KNN based lead-free ceramics with the composition $(1-x)(K_{1-y}Na_y)NbO_3$-$x(Bi_{1/2}Na_{1/2})ZrO_3$ were successfully prepared by a conventional solid-state route. With the increase in BNZ content, the phase structure of KNN gradually transformed from O to mixed R-T and then R phase, indicative of the construction of an R-T based MPB with $0.045 \leq$ BNZ ≤ 0.05 and $0.4 \leq$ Na ≤ 0.7. Optimum ferroelectric, piezoelectric, and strain properties were obtained for the MPB compositions with P_r, d_{33}, k_p, S, and d^*_{33} of 24 $\mu C/cm^2$, 320 pC/N, 48%, 0.168%, and 420 pm/V, respectively. However, despite these attractive room-temperature values at the MPB, there is a dramatic decrease in properties with temperature indicating the MPB is not temperature independent unlike in PZT. Hence there are concerns about the viability of these compositions for high-temperature or high field applications.

Acknowledgments

The authors thank Dr. Haixue Yan from Queen Mary University of London for the helpful discussion. We acknowledge the Sustainability and Substitution of Functional Materials and Devices EPSRC (EP/L017563/1) and the National Natural Science Foundation of China (51402005) for funding and supporting this work. AK and FH acknowledge Abdul Wali Khan University Mardan & NED University of Engineering and Technology for funding respectively.

References

[1]B. Jaffe, W. R. Cook, and H. Jaffe, *Piezoelectric Ceramics*. Academic Press, London, New York City, New York, 1971.
[2]G. H. Haertling, "Ferroelectric Ceramics: History and Technology," *J. Am. Ceram. Soc.*, **82**, 797–818 (1999).
[3]D. Damjanovic, "Ferroelectric, Dielectric and Piezoelectric Properties of Ferroelectric Thin Films and Ceramics," *Rep. Prog. Phys.*, **61**, 1267–324 (1998).
[4]T. R. Shrout and S. Zhang, "Lead-Free Piezoelectric Ceramics: Alternatives for PZT," *J. Electroceram.*, **19**, 113–26 (2007).
[5]R. Guo, L. E. Cross, S. -E. Park, B. Noheda, D. E. Cox, and G. Shirane, "Origin of the High Piezoelectric Response in $PbZr_{1-x}Ti_xO_3$," *Phys. Rev. Lett.*, **84**, 5423–6 (2000).
[6]EU-Directive 2002/96/EC, "Waste Electrical and Electronic Equipment (WEEE)," *Off. J. Eur. Union*, **46**, 24–38 (2003).
[7]EU-Directive 2002/95/EC, "Restriction of the Use of Certain Hazardous Substances in Electrical and Electronic Equipment (RoHS)," *Off. J. Eur. Union*, **46**, 19–23 (2003).
[8]J. Rödel, K. G. Webber, R. Dittmer, W. Jo, M. Kimura, and D. Damjanovic, "Transferring Lead-Free Piezoelectric Ceramics Into Application," *J. Eur. Ceram. Soc.*, **35**, 1659–81 (2015).
[9]M. D. Maeder, D. Damjanovic, and N. Setter, "Lead Free Piezoelectric Materials," *J. Electroceram.*, **13**, 385–92 (2004).
[10]J. Rodel, W. Jo, K. T. P. Seifert, E. M. Anton, T. Granzow, and D. Damjanovic, "Perspective on the Development of Lead-Free Piezoceramics," *J. Am. Ceram. Soc.*, **92**, 1153–77 (2009).
[11]A. Safari and M. Abazari, "Lead-Free Piezoelectric Ceramics and Thin Films," *IEEE Trans. Ultrason. Ferroelectr. Freq. Control*, **57**, 2165–76 (2010).
[12]T. Takenaka and H. Nagata, "Current Status and Prospects of Lead-Free Piezoelectric Ceramics," *J. Eur. Ceram. Soc.*, **25**, 2693–700 (2005).
[13]D. Q. Xiao, J. G. Wu, L. Wu, J. G. Zhu, P. Yu, et al., "Investigation on the Composition Design and Properties Study of Perovskite Lead Free Piezoelectric Ceramics," *J. Mater. Sci.*, **19**, 5408–19 (2009).
[14]P. K. Panda, "Review: Environmental Friendly Lead-Free Piezoelectric Materials," *J. Mater. Sci.*, **44**, 5049–62 (2009).
[15]J. G. Wu, D. Q. Xiao, and J. G. Zhu, "Potassium-Sodium Niobate Lead-Free Piezoelectric Materials: Past, Present, and Future of Phase Boundaries," *Chem. Rev.*, **115**, 2559–95 (2015).
[16]J. F. Li, K. Wang, F. Y. Zhu, L. Q. Cheng, and F. Z. Yao, "(K,Na) NbO_3-Based Lead-Free Piezoceramics: Fundamental Aspects, Processing Technologies, and Remaining Challenges," *J. Am. Ceram. Soc.*, **96**, 3677–96 (2013).
[17]L. Egerton and D. M. Dillon, "Piezoelectric and Dielectric Properties of Ceramics in the System Potassium Sodium Niobate," *J. Am. Ceram. Soc.*, **42**, 438–42 (1959).
[18]Y. Saito, H. Takao, T. Tami, T. Nonoyama, K. Takatori, et al., "Lead-Free Piezoceramics," *Nature*, **432**, 84–7 (2004).
[19]E. Cross, "Lead-Free at Last," *Nature*, **432**, 24–5 (2004).
[20]E. Ringaard and T. Wurlitzer, "Lead-Free Piezoceramics Based on Alkali Niobates," *J. Eur. Ceram. Soc.*, **25**, 2701–7 (2005).
[21]K. Wang and J. F. Li, "Low-Temperature Sintering of Li-Modified (K, Na)NbO_3 Lead-Free Ceramics: Sintering Behavior, Microstructure, and Electrical Properties," *J. Am. Ceram. Soc.*, **93**, 1101–7 (2010).
[22]Y. L. Wang, D. Damjanovic, N. Klein, and N. Setter, "High-Temperature Instability of Li- and Ta-Modified (K, Na)NbO_3 Piezoceramics," *J. Am. Ceram. Soc.*, **91**, 1962–70 (2008).
[23]T. A. Skidmore and S. J. Milne, "Phase Development During Mixed-Oxide Processing of a $[Na_{0.5}K_{0.5}NbO_3]_{1-x}$-$[LiTaO_3]_x$ Powder," *J. Mater. Res.*, **22**, 2265–336 (2007).
[24]S. Zhang, H. J. Lee, C. Ma, and X. Tan, "Sintering Effect on Microstructure and Properties of (K,Na)NbO_3 Ceramics," *J. Am. Ceram. Soc.*, **94**, 3659–65 (2011).
[25]Y. Guo, K. Kakimoto, and H. Ohsato, "Phase Transitional Behavior and Piezoelectric Properties of $Na_{0.5}K_{0.5}NbO_3$-$LiNbO_3$ Ceramics," *Appl. Phys. Lett.*, **85**, 4121–3 (2004).
[26]M. Matsubara, T. Yamaguchi, K. Kikuta, and S. Hirano, "Effect of Li Substitution on the Piezoelectric Properties of Potassium Sodium Niobate Ceramics," *Jpn. J. Appl. Phys.*, **44**, 6136–42 (2005).
[27]S. Zhang, R. Xia, and T. R. Shrout, "Modified $Na_{0.5}K_{0.5}NbO_3$ Based Lead-Free Piezoelectrics With Broad Temperature Usage Range," *Appl. Phys. Lett.*, **91**, 132913, 3pp (2007).
[28]E. K. Akdogan, K. Kerman, M. Abazari, and A. Safari, "Origin of High Piezoelectric Activity in Ferroelectric $(K_{0.44}Na_{0.52}Li_{0.04})$-$(Nb_{0.84}Ta_{0.1}Sb_{0.06})O_3$ Ceramics," *Appl. Phys. Lett.*, **92**, 112908, 3pp (2008).
[29]Z. P. Yang, Y. F. Chang, and L. L. Wei, "Phase Transitional Behavior and Electrical Properties of Lead-Free $(K_{0.44}Na_{0.52}Li_{0.04})(Nb_{0.96-x}Ta_xSb_{0.04})O_3$ Piezoelectric Ceramics," *Appl. Phys. Lett.*, **90**, 042911, 3pp (2007).
[30]K. Wang, and J. F. Li, "Domain Engineering of Lead-Free Li-Modified (K,Na)NbO_3 Polycrystals With Highly Enhanced Piezoelectricity," *Adv. Funct. Mater.*, **20**, 1924–9 (2010).
[31]P. Zhao, B. P. Zhang, and J. F. Li, "High Piezoelectric d_{33} Coefficient in Li-Modified Lead-Free (Na,K)NbO_3 Ceramics Sintered at Optimal Temperature," *Appl. Phys. Lett.*, **90**, 242909, 3pp (2007).
[32]D. M. Lin, K. W. Kwok, K. H. Lam, and H. L. W Chan, "Structure and Electrical Properties of $Na_{0.5}K_{0.5}NbO_3$-$LiSbO_3$ Lead-Free Piezoelectric Ceramics," *J. Appl. Phys.*, **101**, 074111, 6pp (2007).
[33]R. P. Wang, H. Bando, T. Katsumata, Y. Inaguma, H. Taniguchi, and M. Itoh, "Tuning the Orthorhombic-Rhombohedral Phase Transition Temperature in Sodium Potassium Niobate by Incorporating Barium Zirconate," *Phys. Status Solidi RRL*, **3**, 142–4 (2009).
[34]B. Y. Zhang, J. G. Wu, X. P. Wang, X. J. Cheng, J. G. Zhu, and D. Q. Xiao, "Rhombohedral-Orthorhombic Phase Coexistence and Electrical Properties of Ta and $BaZrO_3$ Co-Modified (K, Na)NbO_3 Lead-Free Ceramics," *Curr. Appl. Phys.*, **13**, 1647–50 (2013).
[35]R. Zuo, D. Lv, J. Fu, Y. Liu, and L. Li, "Phase Transition and Electrical Properties of Lead Free $(Na_{0.5}K_{0.5})NbO_3$-$BiAlO_3$ Ceramics," *J. Alloys Compd*, **476**, 836–9 (2009).
[36]H. Du, W. Zhou, F. Luo, D. Zhu, S. Qu, et al., "Design and Electrical Properties Investigation of $(Na_{0.5}K_{0.5})NbO_3$-$BiMeO_3$ Lead-Free Piezoelectric Ceramics," *J. Appl. Phys.*, **104**, 034104, 7pp (2008).
[37]C. Zhang, Z. Chen, W. Jia, L. Wang, Y. B. Chen, et al., "Crystal Structures and Electrical Properties of (1-x)$Na_{0.5}K_{0.5}NbO_3$-$XBi_{0.8}La_{0.2}FeO_3$ Lead-Free Ceramics," *J. Alloys Compd*, **509**, 2425–9 (2011).
[38]W. F. Liang, W. J. Wu, D. Q. Xiao, J. M. Zhu, J. G. Zhu, and J. G. Wu, "New Crystallographic Dielectric Phase Boundary in $Na_{0.5}K_{0.5}NbO_3$-Based Lead-Free Ceramics," *Phys. Status Solidi RRL*, **5**, 220–2 (2011).
[39]R. Z. Zuo, and J. Fu, "Rhombohedral-Retragonal Phase Coexistence and Piezoelectric Properties of (NaK)$(NbSb)O_3$-$LiTaO_3$-$BaZrO_3$ Lead-Free Ceramics," *J. Am. Ceram. Soc.*, **94**, 1467–70 (2011).
[40]R. Z. Zuo, J. Fu, S. B. Lu, and Z. K. Xu, "Normal to Relaxor Ferroelectric Transition and Domain Morphology Evolution in (K,Na)$(Nb,Sb)O_3$-$LiTaO_3$-$BaZrO_3$ Lead-Free Ceramics," *J. Am. Ceram. Soc.*, **94**, 4352–7 (2011).
[41]J. Fu, R. Z. Zuo, S. C. Wu, J. Z. Jiang, L. Li, et al., "Electric Field Induced Intermediate Phase and Polarization Rotation Path in Alkaline Niobate Based Piezoceramics Close to the Rhombohedral and Tetragonal Phase Boundary," *Appl. Phys. Lett.*, **100**, 122902, 5pp (2012).
[42]B. Y. Zhang, J. G. Wu, X. J. Cheng, X. P. Wang, D. Q. Xiao, et al., "Lead-Free Piezoelectrics Based on Potassium Sodium Niobate With Giant d_{33}," *ACS Appl. Mater. Interfaces*, **5**, 7718–25 (2013).
[43]C. Liu, D. Q. Xiao, T. Huang, J. G. Wu, F. X. Li, et al., "Composition Induced Rhombohedral-Tetragonal Phase Boundary in $BaZrO_3$ Modified $(K_{0.445}Na_{0.50}Li_{0.055})NbO_3$ Lead-Free Ceramics," *Mater. Lett.*, **120**, 275–8 (2014).
[44]X. P. Wang, J. G. Wu, D. Q. Xiao, J. G. Zhu, X. J. Cheng, et al., "Giant Piezoelectricity in Potassium-Sodium Niobate Lead-Free Ceramics," *J. Am. Chem. Soc.*, **136**, 2905–10 (2014).
[45]X. P. Wang, T. Zheng, J. G. Wu, D. Q. Xiao, J. G. Zhu, et al., "Characteristics of Giant Piezoelectricity Around the Rhombohedral-Tetragonal Phase Boundary in (K,Na)NbO_3-Based Ceramics With Different Additives," *J. Mater. Chem. A*, **3**, 15951–61 (2015).
[46]T. Zheng, J. G. Wu, D. Q. Xiao, and J. G. Zhu, "Strong Piezoelectricity in (1-x)$(K_{0.4}Na_{0.6})(Nb_{0.96}Sb_{0.04})O_3$–$XBi_{0.5}K_{0.5}Zr_{1-y}Sn_yO_3$ Lead-Free Binary System: Identification and Role of Multiphase Coexistence," *ACS Appl. Mater. Interfaces*, **7**, 5927–37 (2015).
[47]T. Zheng, J. G. Wu, D. Q. Xiao, J. G. Zhu, X. J. Wang, and X. J. Lou, "Potassium-Sodium Niobate Lead-Free Ceramics: Modified Strain as Well as Piezoelectricity," *J. Mater. Chem. A*, **3**, 1868–74 (2015).
[48]J. S. Zhou, K. Wang, F. Z. Yao, T. Zheng, J. G. Wu, et al., "Multi-Scale Thermal Stability of Niobate-Based Lead-Free Piezoceramics With Large Piezoelectricity," *J. Mater. Chem. C*, **3**, 8780–7 (2015).

[49]Y. Y. Wang, L. Hu, Q. L. Zhang, and H. Yang, "Phase Transition Characteristics and Associated Piezoelectricity of Potassium-Sodium Niobate Lead-Free Ceramics," *Dalton Trans.*, **44**, 13688–99 (2015).

[50]Z. Wang, D. Q. Xiao, J. G. Wu, M. Xiao, F. X. Li, and J. G. Zhu, "New Lead-Free $(Na_{0.5}K_{0.5})NbO_3$–$X(Bi_{0.5}Na_{0.5})ZrO_3$ Ceramics With High Piezoelectricity," *J. Am. Ceram. Soc.*, **97**, 688–90 (2014).

[51]Standards Committee of the IEEE Ultrasonics, *Ferroelectrics and Frequency Control Society, "IEEE Standard on Piezoelectricity"*. American National Standards Institute, New York City, New York, 1987.

[52]S. Zhang, E. F. Alberta, R. E. Eitel, C. A. Randall, and T. R. Shrout, "Elastic, Piezoelectric, and Dielectric Characterization of Modified $BiScO_3$-$PbTiO_3$ Ceramics," *IEEE Trans. Ultrasonics, Ferroelectr. Freq. Control*, **52**, 2131–9 (2005).

[53]C. Larson and R. B. Von Dreele, "General Structure Analysis System (GSAS)," *Los Alamos National Laboratory Report LAUR*, Los Alamos, 2004.

[54]H. Toby, "EXPGUI, a Graphical User Interface for GSAS," *J. Appl. Cryst*, **34**, 210–3 (2001).

[55]K. Kakimoto, K. Akao, Y. Guo, and H. Ohsato, "Raman Scattering Study of Piezoelectric $(Na_{0.5}K_{0.5})NbO_3$-$LiNbO_3$ Ceramics," *Jpn. J. Appl. Phys.*, **44**, 7064–7 (2005).

[56]Z. Y. Liu, H. Q. Fan, and M. M. Li, "High Temperature Stable Dielectric Properties of $(K_{0.5}Na_{0.5})_{0.985}B_{i0.015}Nb_{0.99}Cu_{0.01}O_3$ Ceramics With Core-Shell Microstructures," *J. Mater. Chem. C*, **3**, 5851–8 (2015).

[57]A. Khesro, R. Boston, I. Sterianou, D. C. Sinclair, and I. M. Reaney, "Phase Transitions, Domain Structure, and Pseudosymmetry in La- and Ti-Doped $BiFeO_3$," *J. Appl. Phys.*, **119**, 054101, 8pp (2016).

[58]I. Levin, and I. M. Reaney, "Nano- and Mesoscale Structure of $Na_{1/2}Bi_{1/2}TiO_3$: A TEM Perspective," *Adv. Funct. Mater.*, **22**, 3445–52 (2012).

[59]I. Levin, I. M. Reaney, E. -M. Anton, W. Jo, J. Rodel, et al., "Local Structure, Pseudosymmetry, and Phase Transitions in $Na_{1/2}Bi_{1/2}TiO_3$-$K_{1/2}Bi_{1/2}TiO_3$ Ceramics," *Phys. Rev. B*, **87**, 024113, 11pp (2013).

[60]C. A. Randall, N. Kim, J. Kucera, W. Cao, and T. R. Shrout, "Intrinsic and Extrinsic Size Effects in Fine-Grained Morphotropic-Phase-Boundary Lead Zirconate Titanate Ceramics," *J. Am. Ceram. Soc.*, **81**, 677–88 (1998).

[61]D. Wang, M. Cao, and S. Zhang, "Investigation of Ternary System $PbHfO_3$-$PbTiO_3$-$Pb(Mg_{1/3}Nb_{2/3})O_3$ With Morphotropic Phase Boundary Compositions," *J. Am. Ceram. Soc.*, **95**, 3220–8 (2012).

[62]F. Chen, Y. H. Li, G. Y. Gao, F. Z. Yao, K. Wang, et al., "Intergranular Stress Induced Phase Transition in $CaZrO_3$ Modified KNN-Based Lead-Free Piezoelectrics," *J. Am. Ceram. Soc.*, **98**, 1372–6 (2015).

[63]Y. Qin, J. Zhang, Y. Tan, W. Yao, C. Wang, and S. Zhang, "Domain Configuration and Piezoelectric Properties of $(K_{0.50}Na_{0.50})_{1-x}Li_x(Nb_{0.80}Ta_{0.20})O_3$ Ceramics," *J. Eur. Ceram. Soc.*, **34**, 4177–84 (2014).

[64]S. Zhang, R. Xia, L. Lebrun, D. Anderson, and T. R. Shrout, "Piezoelectric Materials for High Power, High Temperature Applications," *Mater. Lett.*, **59**, 3471–5 (2005). □